Experimental modal analysis of RC beams strengthened with SHCC subjected to shear under impact strain rates

Tathiana Caram S P Figueiredo, Cassio M R Gaspar, Marcus Hering, Iurie Curosu, Manfred Curbach, Viktor Mechtcherine, Flávio de Andrade Silva

Experimental modal analysis of RC beams strengthened with SHCC subjected to shear under impact strain rates

Tathiana Caram S.P. Figueiredo [a], Cassio M.R. Gaspar [a], Marcus Hering [b], Iurie Curosu [c], Manfred Curbach [b], Viktor Mechtcherine [c], Flávio de Andrade Silva [a,*]

[a] Department of Civil and Environmental Engineering, Pontifícia Universidade Católica do Rio de Janeiro, 22451-900 Rio de Janeiro, Brazil
[b] Institute of Concrete Structures, Technische Universität Dresden, 01062 Dresden, Germany
[c] Institute of Construction Materials, Technische Universität Dresden, 01062 Dresden, Germany

ARTICLE INFO

Keywords:
Dynamic testing
Experimental modal analysis
SHCC
RC-beams
PVA
HDPE
Shear strengthening

ABSTRACT

Strain Hardening Cement-based Composites (SHCC) holds great potential to be a remarkably effective material for shear strengthening of reinforced concrete beams in case of impact scenarios due to its great energy dissipation capability through the formation of multiple very fine cracks (~100 μm of width). The effectiveness of this technique is investigated in the paper at hand through the observation of the changes in the dynamic properties in terms of natural frequencies, mode shapes, and damping ratios. Considering a non-destructive free vibration excitation of the specimens before the experiment (undamaged/intact state) to their condition after the destructive impact of an accelerated steel projectile. In this sense, two types of reinforcement configurations and two types of strengthening layers were investigated: reinforced concrete beams with and without stirrups were strengthened with SHCC made with polyvinyl alcohol (PVA) and ultra-high molecular weight polyethylene (UHMWPE) and tested under increasing levels of kinetic energy varying between 2.1 kJ and 6.4 kJ by using an accelerated impactor inside a drop tower facility. The parameter variation enabled conclusions with respect to the influence of the stirrup reinforcement and the SHCC strengthening contributions in the case of dynamic scenarios.

1. Introduction

Strain-Hardening Cement-based Composites (SHCC), also known as Engineered Cementitious Composites (ECC), are a class of building material that exhibits an enhanced strain capacity (1–5 %) under tension when compared with plain concrete [1–3]. This distinct strain capacity prior to failure localization is related to the formation of very fine multiple cracks (max. 100 μm of width) [4–6], which are controlled by dispersed polymeric microfibers (3–12 mm long), typically employed with volume fractions of 2 %. Although SHCC nomenclature is remitted to its direct-tension behavior, it also displays advantageous performances under compressive and shear stresses, especially with regard to its energy absorption capacity [7,8]. More specifically referred to shear stress states, tensile and compressive principal stresses of even magnitude will be established around 45° [7,9]. Since the compressive strength of cementitious matrices is intrinsically higher than its tensile strength, it is the effectiveness of the crack bridging process of an SHCC that will mostly affect its shear resistance. Additionally, this shear resistance can be improved depending on the boundary conditions, more specifically through restrain [7], promoting the increase of the orthogonal compression parcel during the principal stress rotation [9].

Aside from its outstanding mechanical response, the complete substitution of normal concrete for SHCC in new structures poses as economically unfeasible mainly due to the cost of the fibers [10–12]. However, it holds great potential for applications as external strengthening layers due to SHCC fresh-state properties which enable spraying or lamination techniques [10]. Therein, shotcrete SHCC has already proven to substantially increase the strength and ductility of existing unreinforced load-bearing masonry in case of seismic-like loading [13]. In case of reinforced concrete (RC) elements, SHCC easily overcomes one of the main problems regarding strengthening materials, the bond between the base materials surface and the strengthening layer as long as the properly rough application surface is ensured [14]. It also presents comparatively a much lower cost than the most commonly marketed strengthen materials [12].

RC structures are, in general, in constant deterioration due to erosive

* Corresponding author.
E-mail address: fsilva@puc-rio.br (F. de Andrade Silva).

actions resulting from environmental exposure conditions (volumetric dilatation, moisture, wind, sea air, etc), air pollution (CO_2), and variations on the service loads [15–17]. Quite often this accumulation of damage requires the rehabilitation of the structure to hold its serviceability, commonly adding new concrete covers. In the long-term, it is also to be expected the degradation of these strengthening layers, which unfortunately makes the task of damage detection harder, especially with regard to the state of the substrate, as the strengthening layers impair any visual inspection [15,18]. On the other hand, strengthening layers made of Fiber-Reinforced Polymers (FRP) are subjected to transverse cracking, interlaminar delamination, fiber breakage, fiber–matrix debonding, and cavitation, representing a damage-detection challenge by themselves [15,17–19].

One advantageous technique to detect the damage in cement-based systems is the evaluation of their vibrational response, more specifically their change in mode shapes, natural frequencies, and damping ratios [15,16,20–26]. For instance, it was already reported that undamaged reinforced concrete members display damping values of ~ 0.85 %, while cracked ones can provide larger coefficients, with values varying between 0.5 and 4.0 % [27–29]. Thus, although experimental modal analysis is intrinsically a non-destructive evaluation, it can also be used to assess the residual response of damaged systems when considering an intact referential, thus being useful to evaluate the residual stability provided by strengthening layers [20,30]. The technique consists of measuring the frequency(ies) at which a structural member would oscillate when disturbed by an external stimulus and allowed to vibrate freely [30]. Therefore, its dynamic response comes from an interaction between its inertial and elastic forces, constrained by the undercritically-damped system, which in turn arises from the substrate and reinforcement internal molecular friction, viscosity, and cracking, thus providing an understanding of the structural integrity of the examined specimen, being an important technique of structural health monitoring [25,26,38,39,30–37]. To the best of the authors' knowledge, there are still limited experiments on RC beams subjected to structural damage focusing on impact scenarios, previously and subsequently monitored through vibration analysis to detect the enhancement of deterioration [33,35]. The topic has been even more discreetly addressed on fiber reinforced composites (FRC) structural elements [36,37,39], let alone members strengthened with SHCC.

In this way, this paper presents the second-part analysis of an experimental campaign designed to examine the influence of transversal reinforcement and strengthening layers on the impact resistance and fracture behavior of RC beams [40]. The influence of the strengthening layers made out of SHCC on the intact specimens, as the contribution to their residual performance, were evaluated through the assessment of their modal parameters i.e. mode shapes, natural frequencies, and damping. A total of 24 structural beams were tested. Their experimental modal results were obtained using two independent routines implemented on Matlab (by MathWorks, USA). Comparisons among the experimental results coming from the RC beams with theoretically calculated values and a numerical model implemented on Abaqus (By Dassault Systèmes Simulia, USA) were used to evaluate the agreement of the vibration modes. Finally, the numerical routines implemented on Matlab were extrapolated for the beams strengthened with SHCC, providing the means for a comparative damage evaluation of these specimens. While this research consists of a very special structural case, it represents an important step forward in the understanding of the contribution of SHCC strengthening covers on the impact resistance of existing structures.

2. Materials and methods

The present program entailed the modal evaluation of 24 specimens that were subjected to increasing levels of impact energy varying from 2.1 kJ to 6.4 kJ. Two variations of RC beams with outer dimensions of 0.13 m × 0.28 m × 1.45 m (width × height × length) were studied: the first group considered the specimens without transversal reinforcement whereas the second one with stirrups on a shear reinforcement ratio of 0.53 %. Both variations had the same longitudinal reinforcement ratio of 0.72 %, and a concrete cover of 10 mm. The investigation focused on the improvement of the impact resistance and residual stability through the use of externally applied strengthening layers of SHCC. Eight beams from each reinforcement configuration (without and with stirrups) received a 20 mm thickness layer of two variations of SHCC, totalizing 16 strengthened specimens. The SHCC was applied only on the lateral surfaces using a wooden perimeter frame, thus while the height held the original value of 0.28 m, the width of the strengthened beams was modified from 0.13 m to 0.165 m. More details regarding the experimental program can be found in [40].

2.1. Materials

All the beams were built with the same normal-weight concrete with a water-to-binder ratio (w/b) of 0.35 and a maximum aggregate size of 8 mm. Besides Portland cement type III (42.5 N), a discrete amount of fly ash was also used as a binder for rheological improvement purposes. The mix design by weight is given in Table 1. The mean compressive strength measured on 150 mm cubes was 49.5 MPa (CoV 3.2 %) at 28 days and 50.9 MPa (CoV 3.9 %) at 42 days, which was the average testing age of the beams. The beams were reinforced with Ø8 mm ribbed bars of steel B500S (standard minimum required value $f_y \approx 500$ MPa).

Two types of normal-strength SHCC (compressive strength, $f_{ck} \approx 42$ MPa) were assessed in this study, as already described on [7]; see also Fig. 1. Following previous investigations by the authors, both held a fiber content of 2% in volume [7]. One was produced with polyvinyl alcohol (PVA) fibers (by Kuraray, Japan), and the other with ultra-high molecular weight polyethylene (UHMWPE), shortly referred as PE fibers (by DSM, the Netherlands). The geometric and mechanical properties of these fibers are listed in Table 2.

The compositions of the SHCC made with PVA and PE fibers are practically identical, although the final composites present distinct mechanical properties, i.e. an average Young Modulus of 17.2 GPa and 23.0 GPa, and strain capacity of 1.0% and 2.5% respectively. The mixture was previously developed by the authors Curosu and Mechtcherine [41–44] to ensure proper crack-bridging behavior for PVA-SHCC. Due to PVA inherent hydrophilic properties [45–47], it yields a strong chemical bond with cementitious matrices. The matrix in reference was purposely conditioned to afford limited bond-strength between the fibers and the matrix, therefore reducing the occurrence of fiber-rupture during the pullout process [44].

PE fibers are intrinsically hydrophobic, hence mainly frictionally anchored to cementitious matrices [3]. Consequently, the pullout behavior of PE-SHCC would be favored by the matrix compactness. However, it was chosen to maintain the same matrix, which was primarily developed to PVA-SHCC for comparison purposes with minor adjustments. The modifications were implemented to ensure the proper workability for PE-SHCC since its relative higher aspect ratio represents a drawback in terms of fiber dispersion. The proper rheology was achieved with a small increase in the superplasticizer content and with a combination of higher energy and duration of mixing [44]. Both SHCC compositions are listed in Table 3.

2.2. Test specimens and setup

All the specimens were subject to impact load by using the accelerated configuration of the drop tower facility located at the Otto-Mohr Laboratory of the Technische Universität Dresden [50]. The RC beams were positioned over rollers and vertically braced at ends so that the supports enabled only the rotation in the plane of loading (Fig. 2a). Each brace consisted of a rubber pad fastened by a pair of manually adjusted metallic clamps. The impact load was applied by a flat-nose steel impactor with 100 mm of diameter, 250 mm length, and 14.2 kg of

Table 1
Concrete composition (kg/m^3).

Component	Cement	Fly ash	Coarse aggregate	Fine aggregate	Water	Superplasticizer
Quantity	380	60	762	932	188	2.85

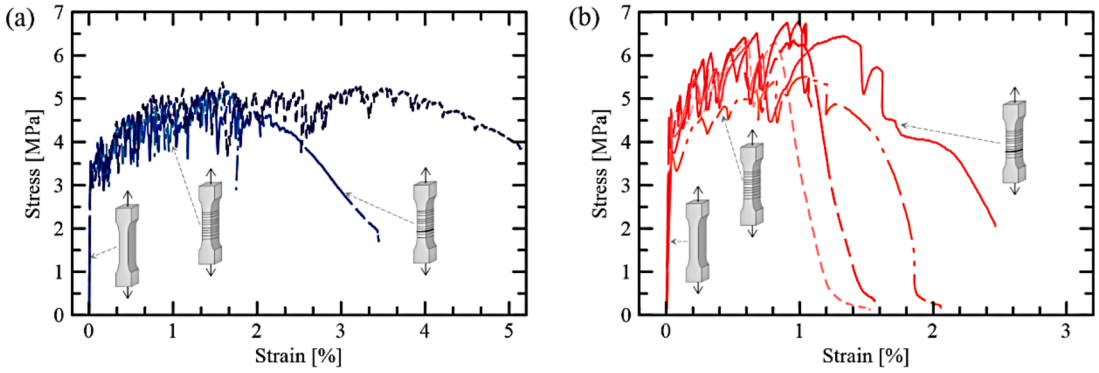

Fig. 1. Direct tensile behavior of the studied SHCC at 28 days: (a) PE-SHCC; (b) PVA-SHCC. Note different scale of the x-axes.

Table 2
Geometric and mechanical properties of PVA and PE fibers according to producers [48,49].

Fiber		PVA	PE
Specification		REC15	SK62
Diameter	[μm]	40	20
Length	[mm]	12	12
Density	[g/cm^3]	1.26	0.97
Tensile strength	[MPa]	1600	2500
Young's modulus	[GPa]	40	80
Elongation at break	[%]	6.0	3.5

Table 3
Compositions of the SHCC under investigation.

	PVA-SHCC [kg/m^3]	PE-SHCC [kg/m^3]
Portland cement CEM I 42.5 R-HS	505	505
Fly ash Steament H4	621	621
Quartz sand 60–200 μm	536	536
Water	338	333
Superplasticizer BASF Glenium ACE 30	10	25
Viscosity modifying agent	4.8	4.8
PVA fiber 2 % by volume	26	–
UHMWPE fiber 2 % by volume	–	20

weight. This projectile was initially charged with pressures varying from 0.2 bar (200 kPa) to 1.2 bar (1200 kPa), resulting in impact velocities from 17.7 m/s to 29.9 m/s, and corresponding to a kinetic energy varying from 2.1 kJ to 6.4 kJ, respectively. The specimens were instrumented with four piezoelectric accelerometers model PCB-M350C04 (by PCB Piezotronics, USA), with a sensitivity of 0.10 mV/(m/s^2), and a bandwidth varying from 0.2 Hz to 25 kHz. The data acquisition system worked on a sampling rate of 200 kHz. Three of the sensors were positioned on the impact front-surface – top of the beams (ACC1, ACC2, and ACC3), and one at the rear-surface – bottom of the beams (ACC4); see Fig. 2b.

The damage assessment was enabled by the modal analysis of the data collected by a non-destructive excitation before and after each test; see Fig. 2c. A metallic half-round impactor head was struck by hand by the same operator in all tests, hitting the specimen always at the same position: on the left front-side of the beam considering the penetration path of the projectile. The data of the accelerometers lasting 2 s in time domain was recorded while the specimens were still clamped on the load cells. It should be noted that only the accelerometer signals (output-only) were considered in the following analysis of Sections 3 and 4.

Fig. 3 relates the nomenclature of the specimens, the pressure and velocity of the steel impactor, and the number of destructive impacts. Most of the beams were subjected to a single event. However, with the intention to assess the residual strength provided by the SHCC layers, additional impacts were performed on some of the strengthened specimens of the intermediate (0.8 bar) series. The specimens were labelled according to their configuration of reinforcement ("WS" and "WOS" in reference to the presence or absence of stirrups, respectively), of the strengthening layer material ("Ref" was used for the reference beams, i.e. specimens without external strengthening, and "PVA" and "PE" indicate the beams which lateral surfaces received the SHCC made with these fibers), and to the initial charging pressure of the impactor (0.2–1.2 bar). Thus, the test set-up results in a total of 116 dynamic responses in terms of acceleration.

3. Analysis methodology

The damage assessment was based on the analysis of the variations of the natural frequencies and damping values of the undamaged and damaged specimens. Both were obtained through the time and frequency domain (TD and FD respectively). The selection of the natural frequencies corresponding to the first three theoretical modes was based on the peaks obtained through FD, on the results of analytical formulations, numerical modeling (Fig. 4a), and supported by the shapes of the normalized modal coordinates (NMC) to unity based only on the TD response (Fig. 4b). Although the results were obtained through two independent protocols, they were intricately related: the peaks visualization was based on an FD routine, as will be further discussed, while the validation data was obtained through TD proceedings. The motivation that drove these parallel studies was the enhancement of reliability on the results.

The analytical evaluation was guided by the expression $f = \mathbb{C}.\pi\sqrt{EI/m'l^4}$ that describes the natural frequency of simply supported beams in Hz [27,29], where EI represents the stiffness of the specimen, being E its Young`s modulus, and I its moment of inertia. The variable m' represents the modal mass of the specimen, which is half the value of its total measured mass in case of simply supported beams, and l is the free span of the set. The variable $\mathbb{C}$ is a constant that assumes the values 0.5,

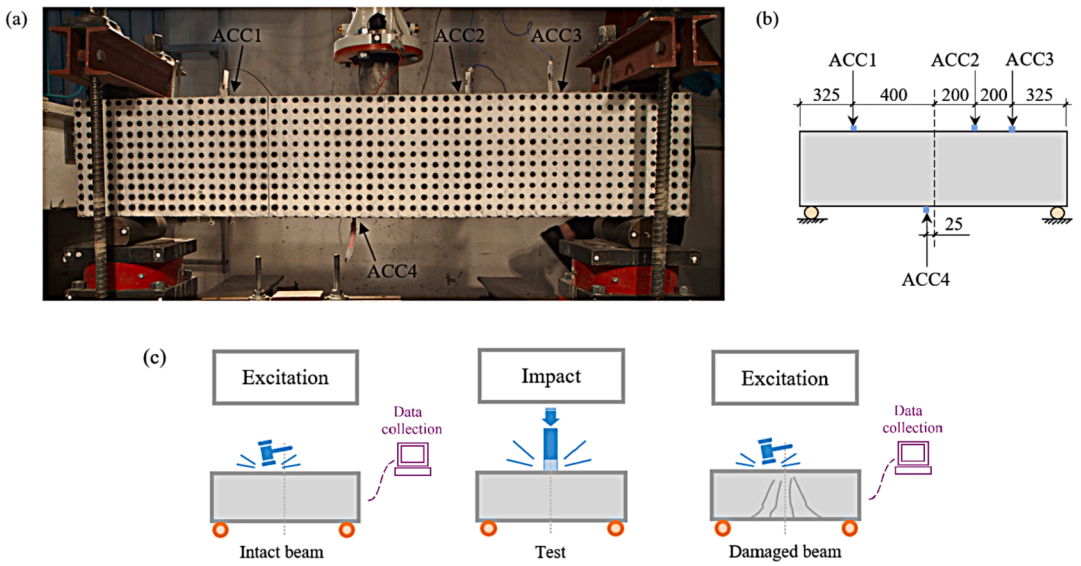

Fig. 2. Test configuration: (a) View of the test set-up; (b) Illustration of the boundary conditions and positioning of the transducers (dimensions in mm); (c) Schematic representation of the measuring steps considered on the experimental modal analysis.

	Acceleration pressure / Impactor´s velocity			
	0.2 bar (17.7 m/s)	**0.4 bar (20.8 m/s)**	**0.8 bar (26.1 m/s)**	**1.2 bar (29.9 m/s)**
Reinforcement	Without stirrups With stirrups	Without stirrups With stirrups	Without stirrups With stirrups	Without stirrups With stirrups
Strengthening	Without	Without PVA-SHCC PE-SHCC	Without PVA-SHCC PE-SHCC	Without PVA-SHCC PE-SHCC
Number of impacts	1 impact	1 impact	1 impact 2, or 3 impacts	1 impact

Fig. 3. Summary of the specimen characteristics and loading conditions.

2.0, or 4.5 for the first, second and third theoretical modes, respectively [27,29].

Analogous to other dynamic evaluations, the detection of the natural frequencies of each specimen is not an easy task, being considerably hampered on the damaged specimens. The calculation by simple observation of the natural period of the TD free vibration response (Fig. 5a) is almost impossible because of the contribution of several vibration modes. Consequently, a Fast Fourier Transformation (FFT) is typically adopted (Fig. 5b). In this sense, a routine was also implemented in Matlab as part of the FD procedures to facilitate the identification of the natural frequencies, easing especially the recognition of the peaks related to the lowest frequencies and the damaged specimens. Thereby, the determination of the natural frequencies was based on the peak values of the Averaged Normalized Power Spectral Density plot (ANPSD) [16,51], which corresponds to the sum of the normalized square magnitude of the spectral density functions obtained from the four accelerometers (see Fig. 5c). For this, the Power Spectral Density (PSD) of each signal was first computed using Welch's method [29]. Additionally, the ANPSD values are also shown in decibels (dB) to improve the visualization of the peaks (Fig. 5d).

Afterward, a combination of low and highpass Butterworth filters to form a bandpass filter was used on the TD signals to isolate the contribution of the vibration modes of interest considering appropriate cutoff frequencies. This procedure allowed the estimation of the modal damping ratios in TD by the automatic curve fitting of the exponential free decay from each accelerometer signal. Furthermore, as each peak in FD was well approximated by a single degree of freedom response, the damping ratios were also determined from the ANPSD plots using the well-known half-power bandwidth method [51,52].

Normalized damage indices based on [32] were also adopted to evaluate the overall cracking progression associated with each impact velocity on the strengthened beams. Damage indexes are a well-known method to qualitatively assess changes in structural modal strain energy of elements without significant variations of the modal mass [16]. The stiffness degradation index (DI_f) was estimated by the change of the natural frequency of a specific vibrational mode of a specimen from its intact state (f_0) and after the damage (f_i): $DI_f = (f_0 - f_i)/f_0$ (1). Analogously, the damping degradation index (DI_ζ) was based on the variation on the damping coefficients of a specimen on its intact (ζ_0) and damaged state (ζ_i) for each vibrational mode: $DI_\zeta = (\zeta_i - \zeta_0)/\zeta_0$ (2).

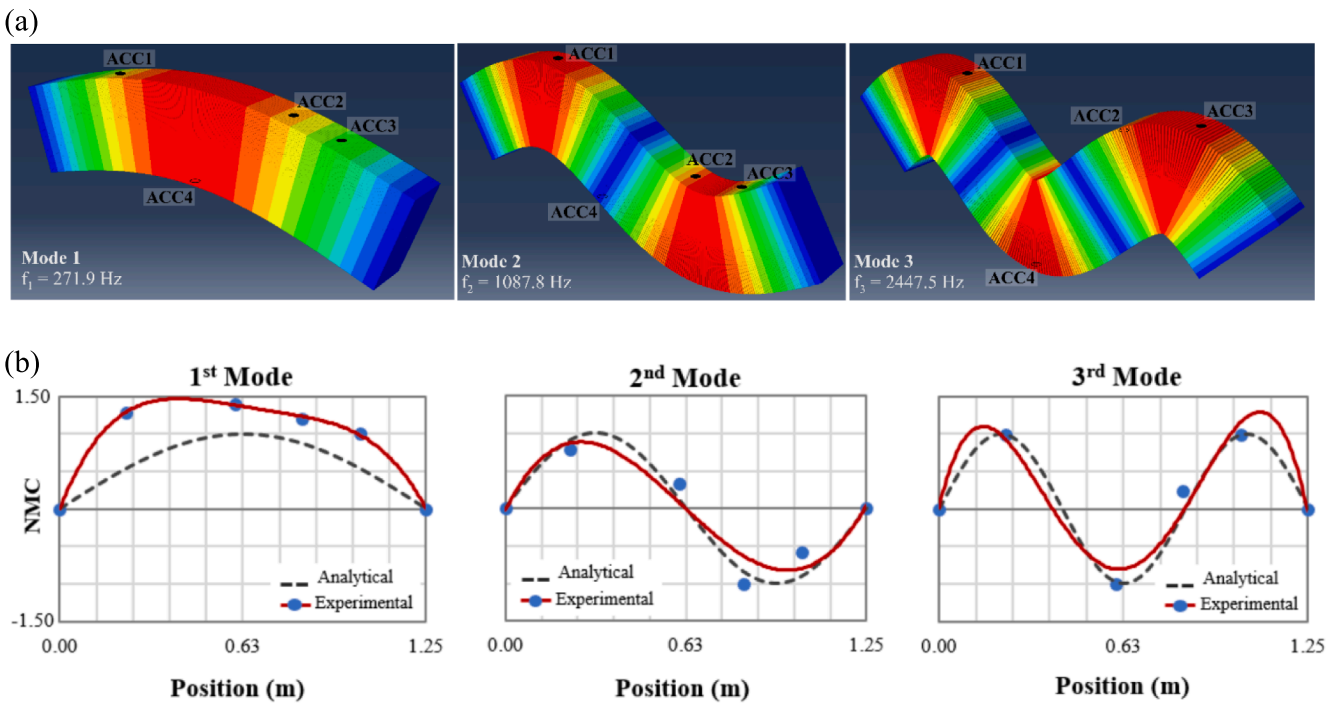

Fig. 4. Three first theoretical vibrational modes with indication of the transducers' positioning (e.g. WOS-Ref): (a) mode shapes and corresponding natural frequencies obtained through numerical modeling; (b) correlation example of the NMC with the analytical formulations.

4. Results and discussion

4.1. RC-beams

Typical vibration spectra of the RC beams coming from the FFT are shown in Fig. 6 before and after the damage. While the peaks referent to the frequencies greater than 500 Hz could be clearly detected, an uncertainty hovered the detection of the first peaks. Thus, as detailed in Section 3, the spectra based on the ANPSD, as part of the FD protocol, were used to support the observations from the TD routine. This way, all the significant peaks until 2000 Hz were initially investigated and the filtered data in the TD was used to plot their NMC. Based on this routine, it was possible to verify for all intact specimens that the peak associated with frequencies around 500 Hz represented an experimental mode without correlation with the first three theoretical vibration modes presented in Fig. 4. These would be spurious modes, that according to the numerical model, would not be able to be performed by real specimens. For this reason, these peaks were not considered in the analysis.

The identified natural frequencies (f) and damping values (ζ) based on the FD and TD to the first three vibration modes are shown in the supplementary Table 4 for the intact beams. As the level of damage does not interfere with the values at this instance (analysis based on the data before the damage), the specimens were grouped into two major groups: specimens without transversal reinforcement (WOS) and specimens with transversal reinforcement (WS). It is possible to notice that the natural frequencies associated with each mode showed a very low dispersion on the results obtained through TD or FD for both WOS (~2.3 %) and WS (~2.7 %) configurations, with the specimens without stirrups presenting superior values for the first (4.7 %), second (1.5 %), and third (1.2 %) modes when compared with the specimens with stirrups. These results point out that although the WS specimens presented a small enhancement of stiffness due to the presence of stirrups, the representativity of the relatively higher amount of reinforcement steel was even more significant in terms of mass, leading to a reduction in the values of the natural frequencies.

As the values of natural frequencies are widely dependent on modal mass of the specimen, stiffness, and boundary conditions, comparisons of the values obtained on the present program with other studies become impractical. Yet, overall benchmarks can be drawn based on the results of the damping coefficients. The undamaged RC beams presented values fairly in agreement with the examined references [27,28], with a maximum dispersion of 52.3% (WS) on the second mode and 36.5% on the third (WOS). However, the values obtained for the first mode deeply contrasted, matching the results of damaged specimens. This behavior is a strong indicator that the first vibrational mode is markedly more controlled by a friction damping, being more affected by the defects (microcracks, voids) intrinsically present on RC members, even under negligible stress states [27]. The second and third modes, in turn, appear to assume a larger portion of the viscous damping typically related to uncracked specimens.

The natural frequencies and damping values according to the first three vibration modes based on the FD and TD analysis for the damaged beams with stirrups considering an impactor speed until 25.73 m/s are available in Table 5. It should be noted that the beams of the WOS configuration, as the WS specimens tested on speeds of 29.9 m/s did not preserve any beam stability, preventing the observation of their modal parameters. As aforementioned, the modal analysis of the damaged specimens in general entailed a great difficulty of identification of the natural frequencies peaks even counting with the ANPSD spectrums (see also Fig. 6b); the dismissed parameters were also related to the acknowledgement of "mixed-mode" NMC plots on the monitored peaks, i.e. it was not possible to clearly distinguish the mode shapes from the theoretical ones.

The parameters referred to the damaged RC beams displayed much more significant dispersion, especially on the damping values, with average values ever exceeding the maximum reference value of 4 % [27,28,53]. It was found a maximum average dispersion of 91.0 % (21.9 m/s), 137.8 % (25.7 m/s), and 45.8 % (25.7 m/s) for the first, second, and third modes, respectively.

The greater damage was observed on the beam subjected to 17.29 m/s of impactor speed, which presented the larger reduction in the natural frequency of the first mode while presenting negligible enhancement on the damping value as would be expected for cracked specimens. This is most probably caused by a greater content of internal defects on this

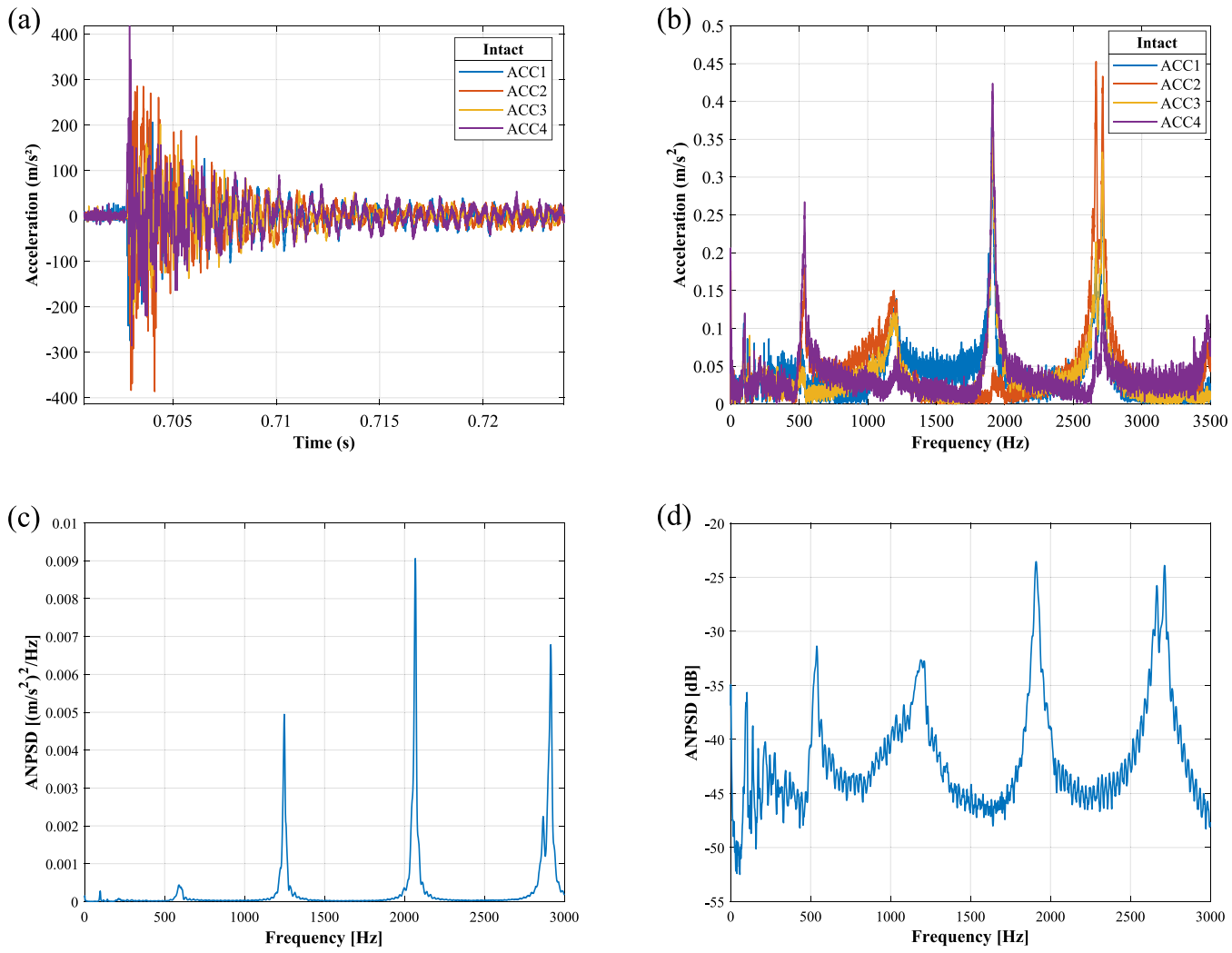

Fig. 5. Typical vibration spectrums for an intact specimen (e.g. WOS-Ref): (a) acceleration-time response considering the four accelerometers; (b) acceleration-frequency response coming from the FFT; (c) ANPSD-frequency response;(d) ANPSD-frequency response on decibel scale.

beam due to problems during the specimen production, which led to an intact state internally much more impaired than what was expected by visual inspection. Indeed, this specimen already presented a natural frequency for the first mode on the intact state quite below the average (7.3 %), representing a reduction of 18.4 % while on the damaged state. This reduction, as of the other specimens here referred, will be better illustrated on the next section.

4.2. RC-beams strengthened with SHCC

The analysis of the strengthened specimens followed the same protocol as the reference beams. The values were listed on Table 6 to 8, so that they were sorted by type of reinforcement and strengthening. As well as the RC beams, the intact strengthened specimens also entailed an uncertainty regarding the detection of the peaks lower than 500 Hz (Fig. 7), justifying the auxiliary plot of the spectrums based on the ANPSD. At first, all significant peaks were monitored. Only when identified a resemblance between an NMC shape and one of the first three theoretical modes, that the peak was properly labeled.

The intact strengthened beams also presented an experimental mode without correlation with the first three theoretical vibration modes on the peak associated with the frequencies around 500 Hz. In fact, when comparing the correspondent natural frequencies of the peaks selected through NMC of the reference specimens (RC beams) with the ones that received the SHCC layers, it is possible to observe that these values corresponding to the three vibration modes are similar to each other, as shown in Fig. 8. This finding indicates that the SHCC initially only slightly affects the natural frequencies of the intact beams.

In turn, the SHCC contribution could be fully noticed after the damage. Although the specimens displayed increased cracking with the enhancement of the impact energy, the strengthening contributed to the maintenance of the values of natural frequencies after the impact, even for the highest levels of damage (impactor speed of 29.9 m/s) on the three monitored vibrational modes; see Fig. 9. This observation agrees with the residual stability observed on the specimens that received the SHCC layers [40], and is a strong indicator of limited progression of damage [32]. On the non-strengthened specimens, none of the RC beams without stirrups outlasted any level of impact, and some specimens with stirrups withstood some vibrational response even if with the substantial average reduction of 37 % on the values of natural frequencies. In contrast, almost all the strengthened beams overcame the reference values (WOS-PVA, 25.0 %; WS-PVA, 23.5 %; WS-PE, 24.7 %) corresponding to damaged RC beams with stirrups (see also Table 4), except for the beams without stirrups strengthened with PE-SHCC, which seemed to present a higher density of cracks though with a smaller opening width [40]. This higher global deformation most probably impaired the WOS-PE specimens internal integrity, and thus their vibrational response on Mode 2 (see Fig. 9b) resulting in an average

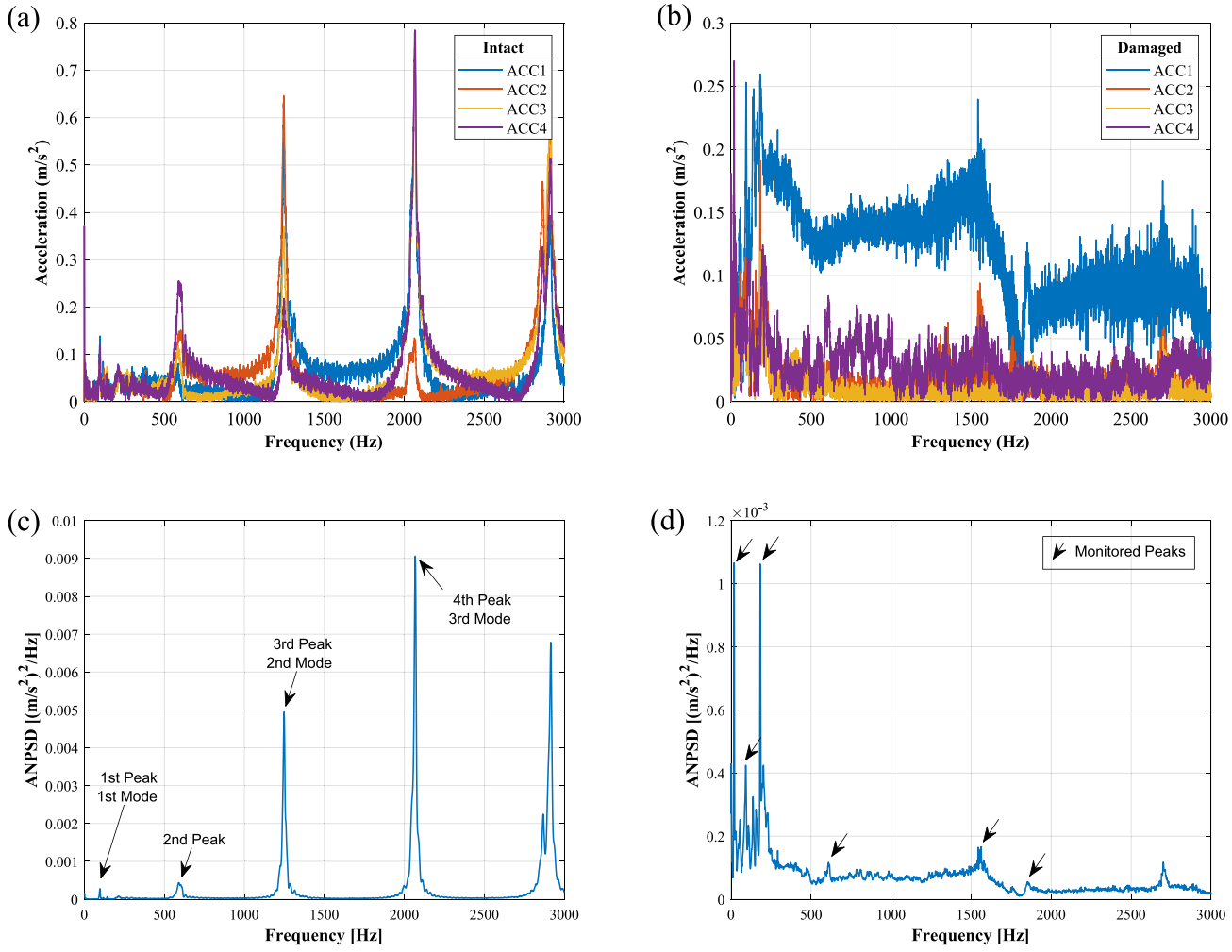

Fig. 6. Typical vibration spectra for the RC specimens and natural frequencies associated with the three first vibrational modes (e.g. WOS-Ref): (a) FFT before the impact; (b) FFT after the impact; (c) ANPSD before the impact; (d) ANPSD after the impact.

Table 4
Natural frequencies and damping values of the undamaged RC beams obtained through TD and FD for the first three theoretical modes regarding the specimens without transversal reinforcement (WOS) and specimens with transversal reinforcement (WS). Standard-deviation in parenthesis.

	f,FD_1 [Hz]	f,TD_1 [Hz]	ζ,FD_1 [%]	ζ,TD_1 [%]	f,FD_2 [Hz]	f,TD_2 [Hz]	ζ,FD_2 [%]	ζ,TD_2 [%]	f,FD_3 [Hz]	f,TD_3 [Hz]	ζ,FD_3 [%]	ζ,TD_3 [%]
WOS	97.78	93.54	5.08	3.28	1210.23	1215.91	0.82	1.14	2016.23	2001.30	0.50	0.57
	(7.32)	(6.78)	(2.57)	(1.39)	(25.52)	(27.51)	(0.29)	(0.48)	(39.75)	(57.21)	(0.09)	(0.04)
WS	94.71	87.96	6.43	5.77	1196.10	1194.84	1.10	1.49	1988.30	1982.41	0.65	0.84
	(6.84)	(2.65)	(1.62)	(1.45)	(26.49)	(25.85)	(0.34)	(0.79)	(36.34)	(35.92)	(0.07)	(0.14)

Table 5
Natural frequencies and damping values of the damaged RC beams with stirrups obtained through TD and FD for the first three theoretical modes.

Speed [m/s]	Mode 1				Mode 2				Mode 3			
	f,FD 1 [Hz]	f,TD 1 [Hz]	ζ,FD 1 [%]	ζ,TD 1 [%]	f,FD 2 [Hz]	f,TD 2 [Hz]	ζ,FD 2 [%]	ζ,TD 2 [%]	f,FD 3 [Hz]	f,TD 3 [Hz]	ζ,FD 3 [%]	ζ,TD 3 [%]
17.29	74.84	–	3.78	–	–	–	–	–	–	–	–	–
21.79	79.48	79.42	7.16	8.11	539.57	530.98	3.33	8.63	1338.70	1336.20	1.41	4.33
25.73	88.19	88.98	7.47	3.74	235.46	242.18	7.48	11.53	1169.50	1030.90	1.66	10.00

global decrease of 46.4 %, even if no significant deterioration could be optically observed.

The maintenance of the values of natural frequencies, as the level of deterioration of the specimens, is antagonistic to the enhancement of the damping coefficient values since the cracking process usually enlarges a structural element's capacity to absorb energy through the development of elastic and plastic (new surfaces, for cement-based materials) deformations [27]. Therefore, not surprisingly the RC specimens with

Table 6
Natural frequencies and damping values of the intact strengthened beams obtained through TD and FD for the first three theoretical modes.

	f,FD_1 [Hz]	f,TD_1 [Hz]	ζ,FD_1 [%]	ζ,TD_1 [%]	f,FD_2 [Hz]	f,TD_2 [Hz]	ζ,FD_2 [%]	ζ,TD_2 [%]	f,FD_3 [Hz]	f,TD_3 [Hz]	ζ,FD_3 [%]	ζ,TD_3 [%]
WOS-PVA	98.13	87.64	3.03	2.73	1159.43	1156.99	1.54	1.83	1908.63	1906.96	0.55	0.68
	(1.59)	(15.85)	(1.15)	(0.81)	(4.19)	(1.71)	(0.29)	(0.48)	(10.69)	(12.97)	(0.10)	(0.06)
WOS-PE	98.30	109.05	4.92	2.49	1168.13	1166.91	1.46	1.75	1906.35	1904.58	0.61	1.10
	(1.39)	(19.66)	(1.89)	(1.56)	(15.88)	(18.83)	(0.80)	(1.10)	(11.94)	(12.34)	(0.08)	(0.96)
WS-PVA	97.81	93.09	3.25	2.67	1140.05	1138.39	1.37	1.59	1878.75	1877.48	0.63	0.84
	(2.75)	(7.34)	(0.67)	(1.63)	(19.42)	(18.85)	(0.17)	(0.39)	(26.43)	(26.30)	(0.11)	(0.22)
WS-PE	92.69	91.83	4.19	3.26	1142.90	1140.74	1.21	1.31	1879.33	1875.91	0.54	1.57
	(4.23)	(10.08)	(1.25)	(1.49)	(4.85)	(4.84)	(0.36)	(0.18)	(7.71)	(9.52)	(0.16)	(1.17)

Table 7
Natural frequencies of the damaged strengthened beams for the first three theoretical modes.

Configuration	Speed [m/s]	f,FD_1 [Hz]	f,TD_1 [Hz]	f,FD_2 [Hz]	f,TD_2 [Hz]	f,FD_3 [Hz]	f,TD_3 [Hz]
WOS-PVA	21.41	85.09	86.25	700.08	–	1374.80	1380.10
	26.30	87.28	85.61	572.80	565.84	1281.05	1220.33
		(1.31)	(4.39)	(16.88)	(17.44)	(150.40)	(141.32)
	29.85	81.66	81.16	–	–	–	–
WOS-PE	20.38	82.92	83.69	660.28	656.37	1197.10	1246.10
	25.33	80.50	76.09	434.84	430.28	1192.00	1184.10
		(3.13)	(8.73)	(142.55)	(136.15)	–	–
	29.90	88.46	88.97	330.33	320.75	1615.00	1559.45
WS-PVA	20.02	98.34	91.27	778.28	772.64	1437.70	1432.95
	26.26	89.61	77.62	679.70	658.44	1372.60	1375.80
		(3.18)	(10.30)	(50.53)	(32.56)	–	–
	29.45	86.98	87.14	675.34	672.04	1390.10	1381.70
WS-PE	20.54	81.98	70.16	699.32	691.27	1743.00	1740.40
	25.71	87.30	87.23	641.01	633.95	1263.90	1283.75
		(7.48)	(7.53)	(6.46)	(3.38)	–	–
	29.90	86.98	87.04	675.34	672.54	1394.90	1383.30

Table 8
Damping values of the damaged strengthened beams for the first three theoretical modes.

Configuration	Speed [m/s]	ζ,FD_1 [%]	ζ,TD_1 [%]	ζ,FD_2 [%]	ζ,TD_2 [%]	ζ,FD_3 [%]	ζ,TD_3 [%]
WOS-PVA	21.41	5.48	4.08	3.23	–	1.38	3.25
	26.30	4.88	2.57	3.20	4.73	1.50	6.89
		(0.91)	(0.04)	(0.25)	(0.30)	(0.21)	(0.88)
	29.85	3.78	3.77	–	–	–	–
WOS-PE	20.38	10.56	6.56	5.53	7.07	10.05	8.96
	25.33	4.16	2.94	3.64	5.88	1.33	3.83
		(0.63)	(0.31)	(0.44)	(0.46)	–	–
	29.90	3.77	2.38	2.15	3.07	1.04	9.83
WS-PVA	20.02	4.57	1.54	1.00	3.18	0.49	3.19
	26.26	6.43	5.15	2.53	4.02	1.34	2.30
		(0.49)	(0.93)	(0.04)	(1.15)	–	–
	29.45	3.33	1.56	2.59	4.62	1.66	4.24
WS-PE	20.54	7.22	7.24	3.28	4.97	1.56	4.22
	25.71	3.99	2.22	2.72	4.17	1.49	2.53
		(0.25)	(0.41)	(0.12)	(0.11)	–	–
	29.90	3.33	1.45	2.59	4.62	1.37	4.32

stirrups, notably the ones that poorly outlasted the impact events, presented the greatest increase in the global damping coefficient (55.2 %), which takes into account only the values corresponding to an established vibrational performance on the undamaged and damaged states; see Table 9. Nevertheless, with the exception of the WOS-PVA specimens that presented a discrete increase in this value (14.8 %) attributed to the rapid crack localization of the strengthening layers observed on these specimens [40], the beams of the remaining configurations displayed substantial enhancements on the same parameter (WOS-PE, 55.4%; WS-PVA, 40.3 %; WS-PE, 43.9%), notoriously without compromising their residual stability; see [40]. From these findings it is clear that PVA-SHCC is more sensitive to the internal reinforcement configuration since the absence of stirrups seemed to jeopardize the internal stresses path. PE-SHCC appeared to better hold the transferred energy, presenting an extremely dense cracking pattern with cracks of small width while the substrate presented itself with severe levels of deterioration [40].

Another outstanding contribution of the SHCC strengthening layers was its participation concerning the modal parameters maintenance while ensuring residual structural stability in the occasion of multiple impact events. As presented in Fig. 10, the strengthened beams were able to repeatedly endure average impact energies of 4.8 kJ. The values of natural frequencies on the undamaged state (0 impacts) are compared with the values obtained after 1, 2, and 3 impacts. The dotted reference values emphasize the magnitude of the natural frequencies of the reference specimens with stirrups, the only RC-only configuration that displayed residual vibrational response after one impact event. Despite the reduction of the natural frequencies associated with the three analytical vibrational modes, especially pronounced for the second and

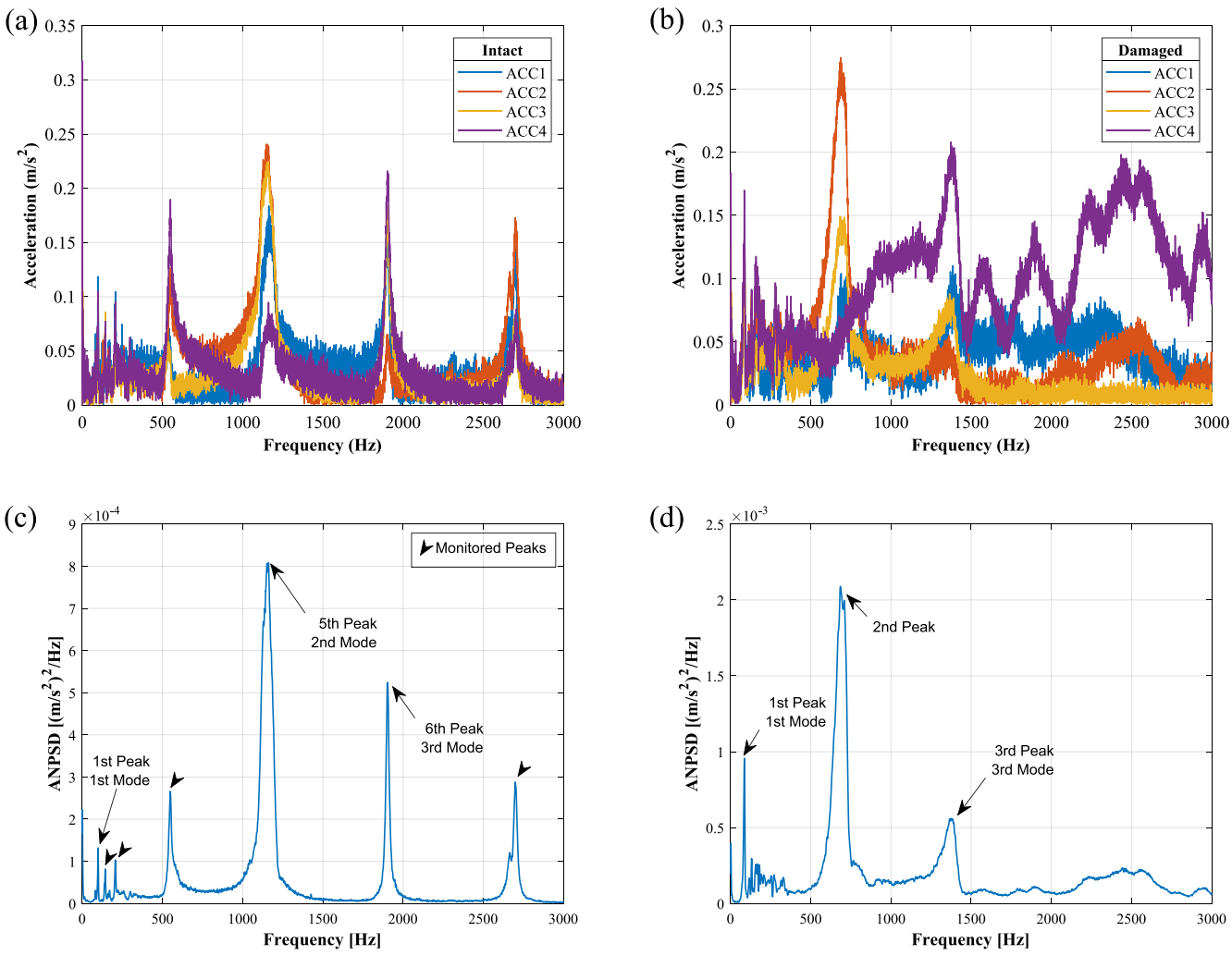

Fig. 7. Typical vibration spectra for the strengthened specimens and natural frequencies associated with the three first vibrational modes (e.g. WOS-PVA): (a) FFT before the impact; (b) FFT after the impact; (c) ANPSD before the impact; (d) ANPSD after the impact.

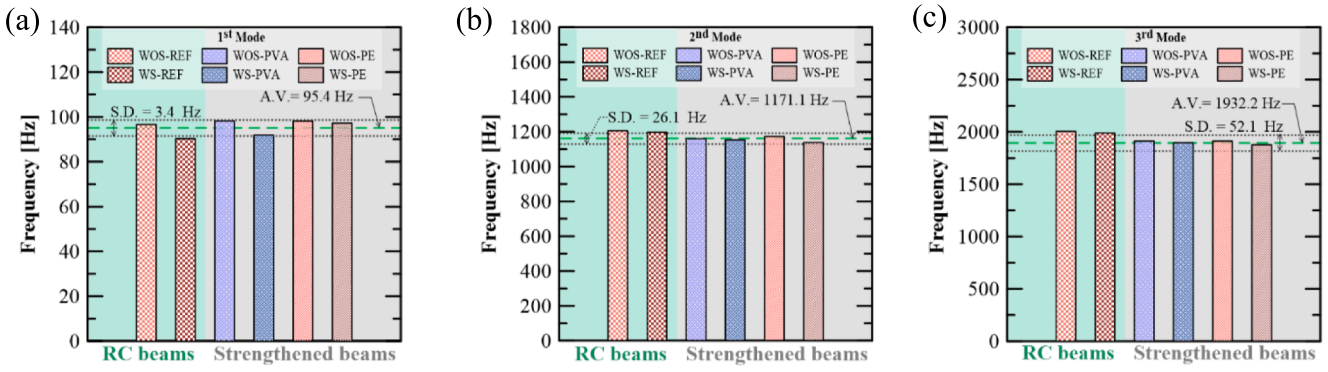

Fig. 8. Average values (A.V.) and standard-deviation (S.D.) of the natural frequencies obtained through TD and FD on the intact specimens classified by type: (a) Mode 1; (b) Mode 2; (c) Mode 3. Note different y-axes.

third modes, it is notorious the afterlife capability provided by the strengthening layers. Emphasis is given to PE-SHCC which was able to stand up to two additional impact events on the WS configuration.

As illustrated in Fig. 11, the values of the average damping coefficients displayed the opposite tendency, significantly increasing with the additional impact events. The results tended to exceed the regular reference value of 4 % related to building beams [27,28], almost achieving levels ~ 10% associated to beam-slabs usable in bridges when subjected to cyclic loading [53]. The configuration WOS-PE exhibited the highest global level of damping when comparing the three modes, enhancing the damping coefficient on 144 % after the first impact, and an additional 107 % after the second, when the level of deterioration detected by visual inspection was considered overly substantial and the loading was interrupted. Both configurations of internal reinforcement

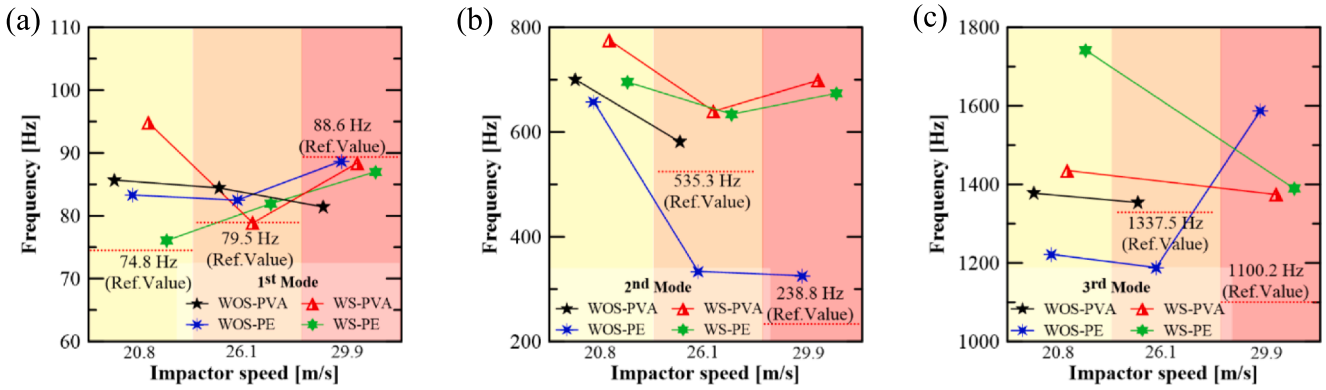

Fig. 9. Average values of the natural frequencies obtained through TD and FD in function of the impactor speed regarding the SHCC damaged specimens classified by type: (a) Mode 1; (b) Mode 2; (c) Mode 3. Note different y-axes. Values on the x-axis are out of phase to improve the visualization. The reference values (Ref. Value) corresponds to the average value obtained on the damaged RC beams with stirrups (WS-Ref; see also Table 5).

Table 9
Stiffness degradation (DI_f) and damping degradation (DI_ξ) indices.

Specimen variation	Impact speed [m/s]	DI_f [%]			DI_ξ [%]		
		Mode 1	Mode 2	Mode 3	Mode 1	Mode 2	Mode 3
WOS-PVA	20.7	−3.9	39.6	27.6	86.3	−9.5	287.4
	25.9	2.5	51.7	39.4	78.9	178.3	627.0
	29.8	17.1	–	–	22.7	–	–
WS-PVA	20.7	−4.4	31.5	23.3	−33.9	75.3	107.6
	25.9	19.4	44.5	–	187.9	108.8	–
	29.8	5.3	41.8	27.1	−13.7	175.2	374.8
WOS-PE	20.7	29.5	44.4	36.1	122.4	109.0	493.0
	25.9	24.5	54.7	–	−38.0	256.9	–
	29.8	9.3	72.2	17.1	16.4	150.2	794.7
WS-PE	20.7	21.8	38.9	7.0	72.5	179.3	58.4
	25.9	3.8	44.8	–	−35.8	145.5	–
	29.8	0.9	40.8	26.5	4.7	236.5	386.1

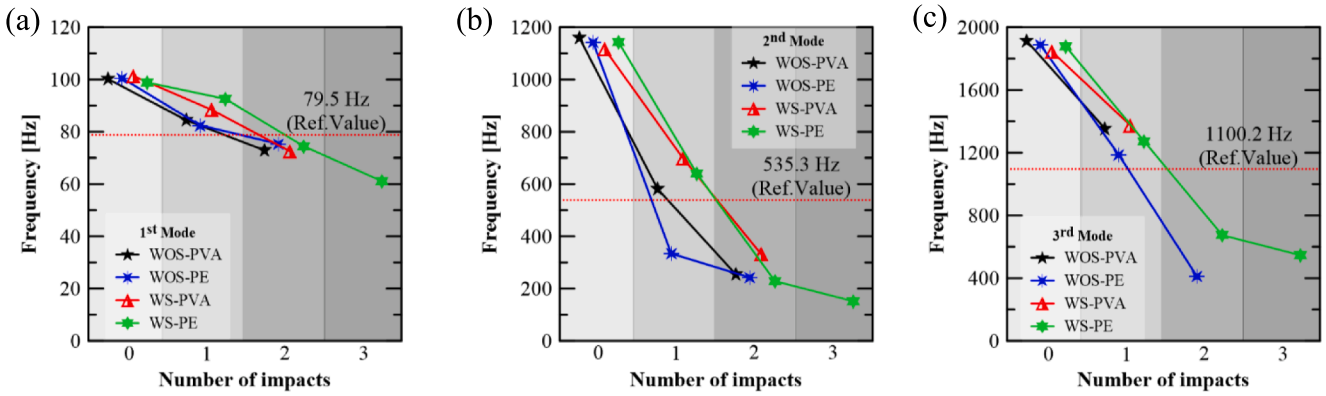

Fig. 10. Average values of the natural frequencies of the SHCC specimens subjected to more than one impact at the speed of 26.1 m/s: (a) Mode 1; (b) Mode 2; (c) Mode 3. Note different y-axes. Values on the x-axis are out of phase to improve the visualization.

which specimens were strengthened with PVA-SHCC held a similar performance, presenting an increase in the damping coefficient of 92 % and 112 % on the first impact event, and 15 % compared to 7 % on the second event for WOS-PVA and WS-PVA, respectively. The configuration WS-PE, that was able to endure more events, displayed a mildly discrete increase on the same parameter presenting enhancements of 60 %, 84 %, and 19 % from the undamaged state to the first, second, and third impact events, respectively.

The analysis of the damage indices [see Eqs. (1) and (2)] enabled a better assessment of the overall behavior of the tested specimens. These values were summarized in Table 9, where the absent values correspond to combinations where no vibrational response could be detected after the damage, preventing the determination of the indices. Positive values of both indices indicate the expected increase in the progression of structural damage, while negative values suggest a pseudo global hardening surely associated with the multiple-cracking process of the SHCC strengthening covers. In accordance with the reference [32] the results of the RC beams displayed a crescent correlation between the level of damage (i.e., impactor velocity) and the indices values in all the monitored vibrational modes. The results coming from the strengthened beams presented meaningful distinctions. In general, the strengthened beams displayed similar values of DI_f for all levels of damage, specially

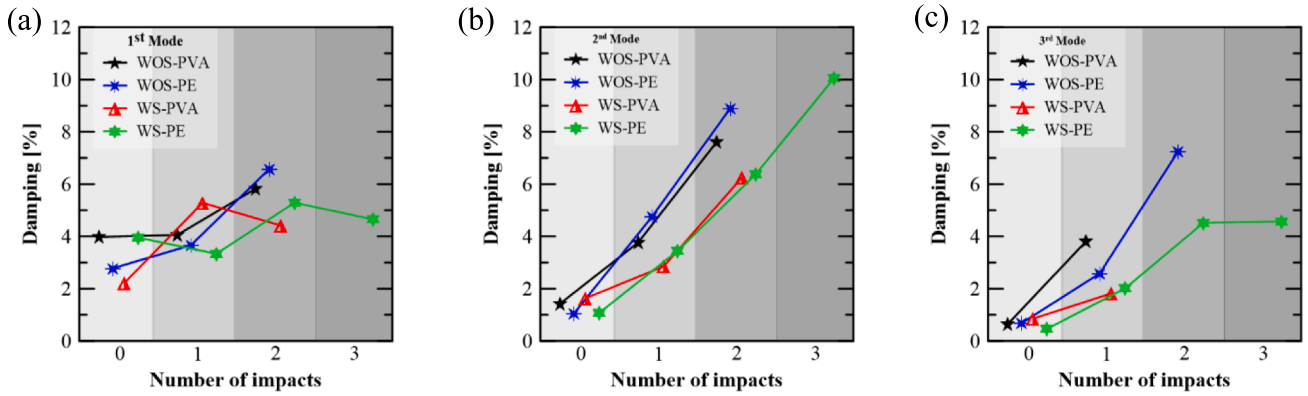

Fig. 11. Average values of damping on the specimens subjected to more than one impact at the speed of 26.1 m/s: (a) Mode 1; (b) Mode 2; (c) Mode 3. Note different y-axes. Values on the x-axis are out of phase to improve the visualization.

considering the second and third vibrational modes. These values are on average 30.8 % below the reference specimens (WS-Ref). Although the indexes of the strengthened specimens could not be directly compared with the results obtained for the RC-beams, as these specimens displayed a sizable mass loss during the impact event [40], these results are a strong indicator on the inferior reduction of stiffness on the beams strengthened with SHCC. The DI_f values related to the first mode presented a considerable variation for the beams strengthened with PVA-SHCC; while it seems to be a small stiffness disturbance, no conclusions could be drawn for certain. In contrast, the specimens strengthened with PE-SHCC tended to display higher values of stiffness degradation for the first mode than the reference specimens, even if with smaller values on the WS configuration. This could be an indication that this composite significantly contributed to the beams' global hardening during the impact event, an assumption backed by the reduction observed on the DI_ζ parameter.

5. Conclusions

A modal analysis was carried out to investigate experimentally the changes in the dynamic properties of 24 full-sized RC beams subjected to impact. The program entailed the examination of the acceleration signals provided by four accelerometers installed in each specimen, assessing a combination of variables such as two configurations of transversal steel reinforcement, two configurations of shear strengthening layers made with SHCC, and increasing levels of kinetic energy varying between 2.1 kJ and 6.4 kJ. Based on the presented results, the following conclusions can be drawn:

1. The internal transversal reinforcement represents a small, but nevertheless relevant influence on the dynamic behavior of RC beams. The RC beams with the total absence of stirrups did not preserve any structural behavior regarding their vibrational response in terms of natural frequencies and vibrational modes after the damage, while the specimens with stirrups withstood a residual dynamic performance until average impact speeds of 4.8 kJ (26.1 m/s), with increased levels of the damping coefficient.
2. In general, the specimens strengthened with SHCC excelled on enduring a residual dynamic response, even standing multiple impact events while preserving the beams modal mass.
3. Both types of SHCC presented a similar dynamic performance when considering the specimens with internal transversal reinforcement. The beams without stirrups strengthened with PVA-SHCC were not able to work out higher frequencies as the ones associated with the third theoretical vibrational mode. Moreover, these specimens did not endure higher levels of impact damage (6.4 kJ, corresponding to the impactor velocity of 29.9 m/s).
4. PE-SHCC appears more suitable for application as strengthening layers of existing structural elements in case of dynamic scenarios where there is a deficient, or content uncertainty, regarding the internal shear reinforcement.

CRediT authorship contribution statement

Tathiana Caram S.P. Figueiredo: Data curation, Writing – original draft, Conceptualization, Formal analysis, Methodology. **Cassio M.R. Gaspar:** Data curation, Formal analysis, Methodology. **Marcus Hering:** Writing – review & editing. **Iurie Curosu:** Writing – review & editing. **Manfred Curbach:** Writing – review & editing. **Viktor Mechtcherine:** Supervision, Funding acquisition, Writing – review & editing, Project administration. **Flávio de Andrade Silva:** Supervision, Funding acquisition, Writing – review & editing, Project administration.

Declaration of Competing Interest

The authors declare that they have no known competing financial interests or personal relationships that could have appeared to influence the work reported in this paper.

Acknowledgments

The investigations presented in this work received the financial support of the German Research Foundation (DFG) in the framework of the Research Training Group GRK 2250 "Mineral-bonded composites for enhanced structural impact safety". The authors also acknowledge the additional financial support provided by the Brazilian agency CNPq (GM/GD 140106/2020-0), and the international cooperation settled between the organizations CAPES (Brazil) and DAAD (Germany) through the Probral program (8887.144079/2017-00). Further thanks are given to the staff of the Alfred-Hütter and Otto-Mohr Laboratories from TUD, where the experimental work was developed.

***Data** availability*

The raw/processed data required to reproduce these findings cannot be shared at this time as the data also form part of ongoing studies.

References

[1] Li VC, Mishra DK, Wu HC. Matrix design for pseudo-strain-hardening fibre reinforced cementitious composites. Mater Struct 1995;28:586–95. https://doi.org/10.1007/BF02473191.
[2] Ma H, Qian S, Zhang Z, Lin Z, Li VC. Tailoring Engineered Cementitious Composites with local ingredients. Constr Build Mater 2015;101:584–95. https://doi.org/10.1016/j.conbuildmat.2015.10.146.

[3] Curosu I, Liebscher M, Mechtcherine V, Bellmann C, Michel S. Tensile behavior of high-strength strain-hardening cement-based composites (HS-SHCC) made with high-performance polyethylene, aramid and PBO fibers. Cem Concr Res 2017;98:71–81. https://doi.org/10.1016/j.cemconres.2017.04.004.

[4] Li VC. On Engineered Cementitious Composites (ECC) - A review of the material and its applications. J Adv Concr Technol 2003;1(3):215–30.

[5] Yao Y, Silva FA, Butler M, Mechtcherine V, Mobasher B. Failure localization and correlation of high-speed tension and impact tests of strain-hardening cement-based composites. J Mater Civ Eng 2017;29:04017212. https://doi.org/10.1061/(ASCE)MT.1943-5533.0002056.

[6] Li VC, Leung CKY. Steady-State and multiple cracking of short random fiber composites. J Eng Mech 1992;118:2246–64. https://doi.org/10.1061/(ASCE)0733-9399(1992)118:11(2246).

[7] Figueiredo TCSP, Curosu I, Gonzáles GLG, Hering M, Silva FA, Curbach M, et al. Mechanical behavior of strain-hardening cement- based composites (SHCC) subjected to torsional loading and to combined torsional and axial loading. Mater Des 2021;198:14. https://doi.org/10.1016/j.matdes.2020.109371.

[8] Li VC. Damage tolerant ECC for integrity of structures under extreme loads. In: Proc 2009 Struct Congr - Don't Mess with Struct Eng Expand Our Role 2009:2209–18. https://doi.org/10.1061/41031(341)242.

[9] van Zijl GPAG. Improved mechanical performance: Shear behaviour of strain-hardening cement-based composites (SHCC). Cem Concr Res 2007;37(8):1241–7.

[10] Huang BT, Li QH, Xu SL, Zhou B. Strengthening of reinforced concrete structure using sprayable fiber-reinforced cementitious composites with high ductility. Compos Struct 2019;220:940–52.

[11] Wei J. Shear strengthening of reinforced concrete beams with High Strength Strain-Hardening Cementitious Composites (HS-SHCC). Mater Struct 2020;53:1–15. https://doi.org/10.21012/fc10.233281.

[12] Li VC. High performance fiber reinforced cementitious composites as durable material for concrete structure repair. Restor Build Monum an Int J 2004;10:163–80.

[13] van Zijl GPAG, de Jager DJA. Improved ductility of SHCC retrofitted unreinforced load bearing masonry via a strip-debonded approach. J Build Eng 2019;24:100722. https://doi.org/10.1016/j.jobe.2019.02.014.

[14] Khalil AEH, Etman E, Atta A, Essam M. Behavior of RC beams strengthened with strain hardening cementitious composites (SHCC) subjected to monotonic and repeated loads. Eng Struct 2017;140:151–63. https://doi.org/10.1016/j.engstruct.2017.02.049.

[15] Sanders DR, Kim YI, Stubbs N. Nondestructive evaluation of damage in composite structures using modal parameters. Exp Mech 1992;32:240–51. https://doi.org/10.1007/BF02319362.

[16] Prado DM, Araujo IDG, Haach VG, Carrazedo R. Assessment of shear damaged and NSM CFRP retrofitted reinforced concrete beams based on modal analysis. Eng Struct 2016;129:54–66. https://doi.org/10.1016/j.engstruct.2016.09.058.

[17] Govindasamy M, Kamalakannan G, Kesavan C, Meenashisundaram GK. Damage detection in glass/epoxy laminated composite plates using modal curvature for structural health monitoring applications. J Compos Sci 2020;4:27. https://doi.org/10.3390/jcs4040185.

[18] Song H, Popovics JS. Characterization of steel-concrete interface bonding conditions using attenuation characteristics of guided waves. Cem Concr Compos 2017;83:111–24. https://doi.org/10.1016/j.cemconcomp.2017.07.001.

[19] Lezgy-Nazargah M, Etemadi E. Reduced modal state-space approach for low-velocity impact analysis of sandwich beams. Compos Struct 2018;206:762–73. https://doi.org/10.1016/j.compstruct.2018.08.081.

[20] Katunin A. Nondestructive damage assessment of composite structures based on wavelet analysis of modal curvatures: state-of-the-art review and description of wavelet-based damage assessment benchmark. Shock Vib 2015;2015:1–19.

[21] Lee KS, Il CJ, Park SE, Hwang JS, Lee BY. Damping property of prepacked concrete incorporating coarse aggregates coated with polyurethane. Cem Concr Compos 2018;93:301–8. https://doi.org/10.1016/j.cemconcomp.2018.06.018.

[22] Yang D, Kang C, Hu Z, Ye B, Xiang P. On the study of element modal strain energy sensitivity for damage detection of functionally graded beams. Compos Struct 2019;224:110989. https://doi.org/10.1016/j.compstruct.2019.110989.

[23] Nasery MM, Hüsem M, Okur FY, Altunişik AC. Numerical and experimental investigation on dynamic characteristic changes of encased steel profile before and after cyclic loading tests. Int J Civ Eng 2020;18:1411–31. https://doi.org/10.1007/s40999-020-00545-0.

[24] Yadav A, Amabili M, Panda SK, Dey T, Kumar R. Nonlinear damped vibrations of three-phase CNT-FRC circular cylindrical shell. Compos Struct 2021;255:112939. https://doi.org/10.1016/j.compstruct.2020.112939.

[25] Hering M, Bracklow F, Scheerer S, Curbach M. Reinforced concrete plates under impact load—damage quantification. Materials (Basel) 2020;13:1–13. https://doi.org/10.3390/ma13204554.

[26] Hering M. Untersuchung von mineralisch gebundenen Verstärkungsschichten für Stahlbetonplatten gegen Impaktbeanspruchungen 2020.

[27] Bachmann H, Ammann WJ, Delschl F, Eisenmann J, Floegl I, Hirsch GH, et al. Vibration problems in structures: Practical guidelines. 1997. https://doi.org/10.1139/l96-116.

[28] Soriano HL. Introdução à Dinâmica das Estruturas. 2014.

[29] Brandt A. Noise and Vibration Analysis. John Wiley and Sons Ltd.; 2011.

[30] Walunj Prashant S, Chougule VN, Mitra AC. Investigation on modal parameters of rectangular cantilever beam using experimental modal analysis. Mater Today Proc 2015;2:2121–30. https://doi.org/10.1016/j.matpr.2015.07.214.

[31] Panteliou SD, Chondros TG, Argyrakis VC, Dimarogonas AD. Damping factor as an indicator of crack severity. J Sound Vib 2001;241:235–45. https://doi.org/10.1006/jsvi.2000.3299.

[32] Othman H, Marzouk H. Dynamic identification of damage control characteristics of ultra-high performance fiber reinforced concrete. Constr Build Mater 2017;157:899–908. https://doi.org/10.1016/j.conbuildmat.2017.09.169.

[33] Bernagozzi G, Mukhopadhyay S, Betti R, Landi L, Diotallevi PP. Output-only damage detection in buildings using proportional modal flexibility-based deflections in unknown mass scenarios. Eng Struct 2018;167:549–66. https://doi.org/10.1016/j.engstruct.2018.04.036.

[34] Andersson A, Östlund J, Ülker-kaustell M, Battini J, Karoumi R. Experimental vibration analysis for civil structures. vol. 5. 2018.

[35] Morgantini M, Betti R, Balsamo L. Structural damage assessment through features in quefrency domain. Mech Syst Signal Process 2021;147:107017. https://doi.org/10.1016/j.ymssp.2020.107017.

[36] Li L, Guo Y, Liu F. Test analysis for FRC beams strengthened with externally bonded FRP sheets. Constr Build Mater 2008;22:315–23. https://doi.org/10.1016/j.conbuildmat.2006.08.016.

[37] Geweth CA, Khosroshahi FS, Sepahvand K, Kerkeling C, Marburg S. Damage detection of fibre-reinforced composite structures using experimental modal analysis. Procedia Eng 2017;199:1900–5. https://doi.org/10.1016/j.proeng.2017.09.128.

[38] Bachoo R, Bridge J. The modal density of composite beams incorporating the effects of shear deformation and rotary inertia. J Sound Vib 2018;423:459–71. https://doi.org/10.1016/j.jsv.2018.01.013.

[39] Li H, Wang Z, Lv H, Zhou Z, Han Q, Liu J, et al. Nonlinear vibration analysis of fiber reinforced composite cylindrical shells with partial constrained layer damping treatment. Thin-Walled Struct 2020;157:107000. https://doi.org/10.1016/j.tws.2020.107000.

[40] Figueiredo TCSP. On the mechanical behavior of strain-hardening cementitious composites (SHCC) under combined and impact loading. Pontifical Catholic Univ Rio de Janeiro 2021.

[41] Curosu I, Pirskawetz S, Mechtcherine V. Characterizing the crack development in strain-hardening cement-based composites (SHCC) by means of acoustic emission. In: Proc Fram Calif 2016:1–10. https://doi.org/10.21012/fc9.207.

[42] Curosu I, Mechtcherine V, Millon O. Effect of fiber properties and matrix composition on the tensile behavior of strain-hardening cement-based composites (SHCCs) subject to impact loading. Cem Concr Res 2016;82:23–35. https://doi.org/10.1016/j.cemconres.2015.12.008.

[43] Curosu I, Mechtcherine V, Forni D, Cadoni E. Performance of various strain-hardening cement-based composites (SHCC) subject to uniaxial impact tensile loading. Cem Concr Res 2017;102:16–28.

[44] Curosu I. Influence of Fiber Type and Matrix Composition on the Tensile Behavior of Strain-Hardening Cement-Based Composites (SHCC) Under Impact Loading. Technischen Universität Dresden (TU Dresden) 2017.

[45] Kanda T, Li VC. Interface Property and Apparent Strength of High-Strength Hydrophilic Fiber in Cement Matrix. J Mater Civ Eng 1998;10(1):5–13.

[46] Li VC, Wu C, Wang S, Ogawa A, Saito T. Interface tailoring for strain-hardening polyvinyl alcohol-engineered cementitious composite (PVA-ECC). ACI Mater J 2002;99:463–72. https://doi.org/10.14359/12325.

[47] Arain MF, Wang M, Chen J, Zhang H. Experimental and numerical study on tensile behavior of surface modified PVA fiber reinforced strain-hardening cementitious composites. Constr Build Mater 2019;217:403–15. https://doi.org/10.1016/j.conbuildmat.2019.05.083.

[48] Kuralon RECS15/RECS100L/RFS400 Standard Properties 2020. http://kuralon-frc.kuraray.com/product-application/for-mortar/recs.

[49] Dyneema D. Ultra high molecular weight polyethylene fiber from DSM Dyneema. Tech DataSheet 2016;49.

[50] La MDE, Du R. Size effect method for determining fracture energy and process zone size of concrete. Int J Rock Mech Min Sci Geomech Abstr 1991;28:A198. https://doi.org/10.1016/0148-9062(91)93225-u.

[51] Felber AJ. Development of a hybrid bridge evaluation system. University of British Columbia; 1993.

[52] Chopra A k. Dynamics of Structures: Theory and Applications to Earthquake Engineering. Prentice-Hall; 2020.

[53] Daneshjoo, F., Gharighoran AE. Investigation of damping in craked concrete beams usable in bridges 2006. https://doi.org/10.13140/RG.2.1.2997.2567.